J|A|C|S ARTICLES

Published on Web 10/12/2010

Dynamic Structural Changes at $LiMn_2O_4$/Electrolyte Interface during Lithium Battery Reaction

Masaaki Hirayama,[†] Hedekazu Ido,[†] KyungSu Kim,[†] Woosuk Cho,[†] Kazuhisa Tamura,[‡] Jun'ichiro Mizuki,[‡] and Ryoji Kanno*,[†]

Department of Electronic Chemistry, Interdisciplinary Graduate School of Science and Engineering, Tokyo Institute of Technology, 4259 Nagatsuta, Midori-ku, Yokohama 226-8502, Japan, and Japan Atomic Energy Agency, Synchrotron Radiation Research Center, Kansai Research Establishment, 1-1-1 Kouto Sayo-cho Sayo-gun, Hyogo 679-5148, Japan

Received July 5, 2010; E-mail: kanno@echem.titech.ac.jp

Abstract: Gaining a thorough understanding of the reactions on the electrode surfaces of lithium batteries is critical for designing new electrode materials suitable for high-power, long-life operation. A technique for directly observing surface structural changes has been developed that employs an epitaxial $LiMn_2O_4$ thin-film model electrode and surface X-ray diffraction (SXRD). Epitaxial $LiMn_2O_4$ thin films with restricted lattice planes (111) and (110) are grown on $SrTiO_3$ substrates by pulsed laser deposition. *In situ* SXRD studies have revealed dynamic structural changes that reduce the atomic symmetry at the electrode surface during the initial electrochemical reaction. The surface structural changes commence with the formation of an electric double layer, which is followed by surface reconstruction when a voltage is applied in the first charge process. Transmission electron microscopy images after 10 cycles confirm the formation of a solid electrolyte interface (SEI) layer on both the (111) and (110) surfaces and Mn dissolution from the (110) surface. The (111) surface is more stable than the (110) surface. The electrode stability of $LiMn_2O_4$ depends on the reaction rate of SEI formation and the stability of the reconstructed surface structure.

1. Introduction

Intercalation reactions are chemical reactions in which guest ions are inserted in and extracted from gaps in a host lattice without significantly modifying the lattice itself. They form the basis of lithium battery operation, which is driven by electrochemical reactions.[1−3] Although there are minimal changes to the lattice during intercalation, restructuring of the lattice is often accompanied by a phase transition, which is one of the factors that determine the kinetics and reversibility of lithium batteries.[4] Structural studies of intercalation materials provide valuable information for developing lithium batteries.

Lithium manganese oxide ($LiMn_2O_4$) is one of the most promising materials for the positive electrodes of large-scale batteries for purely electric vehicles. It is both cheaper and more environmentally friendly than $LiCoO_2$, $LiNiO_2$, and V_6O_{13}.[5,6] The crystal structure of bulk polycrystalline $LiMn_2O_4$ has been extensively investigated by X-ray diffraction (XRD),[7−11] neutron diffraction,[11,12] nuclear magnetic resonance,[13,14] and Raman spectroscopy.[15] $LiMn_2O_4$ has the spinel structure (space group $Fd\bar{3}m$) in which Li and Mn cations respectively occupy tetrahedral (8a) and octahedral (16d) sites in the intervening cubic close-packed array of oxygen atoms (32e sites). The interstitial spaces in the Mn_2O_4 framework can be viewed as a network of tetrahedral 8a sites, which can function as pathways for transporting lithium ions in the structure. The most significant problem with the spinel is capacity fading after extended storage or an electrochemical process; this is particularly problematic at high temperatures.[16] Based on structural observations during electrochemical (de)intercalation and after charge−discharge cycling, two main mechanisms of capacity fading have been proposed: lattice modifications accompanied by the Jahn−Teller

[†] Tokyo Institute of Technology.
[‡] Japan Atomic Energy Agency.

(1) Mizushima, K.; Jones, P. C.; Wiseman, P. J.; Goodenough, J. B. *Mater. Res. Bull.* **1980**, *15*, 783–789.
(2) Kanno, R.; Takeda, Y.; Ichikawa, T.; Nakanishi, K.; Yamamoto, O. *J. Power Sources* **1989**, *26*, 535–543.
(3) Mohri, M.; Yanagisawa, N.; Tajima, Y.; Tanaka, H.; Mitate, T.; Nakajima, S.; Yoshida, M.; Yoshimoto, Y.; Suzuki, T.; Wada, H. *J. Power Sources* **1989**, *26*, 545–551.
(4) Croguennec, L.; Pouillerie, C.; Mansour, A. N.; Delmas, C. *J. Mater. Chem.* **2001**, *11*, 131–141.
(5) Thackeray, M. M.; David, W. I. F.; Bruce, P. G.; Goodenough, J. B. *Mater. Res. Bull.* **1983**, *18*, 461–472.
(6) Thackeray, M. M. *Prog. Solid State Chem.* **1997**, *25*, 1–71.
(7) Gummow, R. J.; Thackeray, M. M. *J. Electrochem. Soc.* **1994**, *141*, 1178–1182.
(8) Liu, W.; Kowal, K.; Farrington, G. C. *J. Electrochem. Soc.* **1998**, *145*, 459–465.
(9) Lee, Y. J.; Wang, F.; Mukerjee, S.; McBreen, J.; Grey, C. P. *J. Electrochem. Soc.* **2000**, *147*, 803–812.
(10) Sun, X.; Yang, X. Q.; Balasubramanian, M.; McBreen, J.; Xia, Y.; Sakai, T. *J. Electrochem. Soc.* **2002**, *149*, A842–A848.
(11) Yonemura, M.; Yamada, A.; Kobayashi, H.; Tabuchi, M.; Kamiyama, T.; Kawamoto, Y.; Kanno, R. *J. Mater. Chem.* **2004**, *14*, 1948–1958.
(12) Yonemura, M.; Kohigashi, T.; Yamada, A.; Sonoyama, N.; Kobayashi, H.; Kamiyama, T.; Kanno, R. *Electrochemistry* **2003**, *71*, 1160–1161.
(13) Lee, Y. J.; Wang, F.; Grey, C. P. *J. Am. Chem. Soc.* **1998**, *120*, 12601–12613.
(14) Grey, C. P.; Dupre, N. *Chem. Rev.* **2004**, *104*, 4493–4512.
(15) Huang, W. W.; Frech, R. *J. Power Sources* **1999**, *82*, 616–620.
(16) Tarascon, J. M.; Armand, M. *Nature* **2001**, *414*, 359–367.

10.1021/ja105389t

effect[5,17] and decomposition of the material itself during charge−discharge cycles.[12]

Studies of crystal structural changes have resulted in a better understanding of the reaction mechanisms in the bulk electrode. However, little is known about the electrochemical reaction at the electrode surface. Although electrochemical and spectroscopic studies have emphasized the importance of surface reactions on the power and calendar-life characteristics,[18,19] the surface reaction mechanism still remains unclear for several reasons. First, the electrode surface is a complicated reaction field at which several processes occur: diffusion of lithium in the electrolyte, adsorption of solvated lithium on the electrode surface, desolvation, surface diffusion, charge transfer, intercalation into the structure, and diffusion in the bulk structure. Second, many factors affect the surface reactions of polycrystalline electrodes, including the surface morphology and the presence of grain boundaries, surface impurities, and surface defects. Third, most experimental methods for investigating the electrode surface are *ex situ* techniques and thus provide interfacial information indirectly. In particular, no experimental techniques have been developed for detecting the surface crystal structure during battery operation.

Epitaxial thin-film electrodes offer the following advantages for clarifying the surface reaction mechanism.[20−22] First, they have very flat surfaces with roughnesses of ∼1 nm; these flat surfaces are ideal interfaces, which simplify surface reactions. Second, the film thickness can be controlled in the range 1−100 nm; a very thin film can function as a surface-enhanced electrode. Third, the reaction field is restricted by the lattice orientation, which can provide information on anisotropic reaction mechanisms. Fourth, flat electrode surfaces may enable surface structural changes to be detected by *in situ* X-ray surface scattering techniques. We have succeeded in detecting the formation of a surface layer and changes in the surface roughness on $LiMn_2O_4$ surfaces using epitaxial $LiMn_2O_4$ thin films and *in situ* X-ray reflectometry. Our results have demonstrated that the stability of the $LiMn_2O_4$ surface depends on the lattice plane.[22] However, no information has been obtained on changes to the crystal structure on $LiMn_2O_4$ surfaces.

In the present study, surface structural changes of $LiMn_2O_4$ during the (de)intercalation process were directly observed by *in situ* surface XRD (SXRD) measurements of epitaxial $LiMn_2O_4$ thin films synthesized on $SrTiO_3$ single-crystal substrates by pulsed laser deposition (PLD). Furthermore, we succeeded in observing changes to the surface structure by *ex situ* transmission electron microscopy (TEM). Drastic changes in the atomic arrangements at the surface occurred during the initial battery process. The lithium intercalation and electrode degradation mechanisms are discussed on the basis of these experimental observations.

(17) Ohzuku, T.; Kato, J.; Sawai, K.; Hirai, T. *J. Electrochem. Soc.* **1991**, *138*, 2556–2560.
(18) Amatucci, G.; Du Pasquier, A.; Blyr, A.; Zheng, T.; Tarascon, J. M. *Electrochim. Acta* **1999**, *45*, 255–271.
(19) Cho, J.; Kim, G. B.; Lim, H. S.; Kim, C. S.; Yoo, S. I. *Electrochem. Solid State Lett.* **1999**, *2*, 607–609.
(20) Hirayama, M.; Sonoyama, N.; Abe, T.; Minoura, M.; Ito, M.; Mori, D.; Yamada, A.; Kanno, R.; Terashima, T.; Takano, M.; Tamura, K.; Mizuki, J. *J. Power Sources* **2007**, *168*, 493–500.
(21) Hirayama, M.; Sakamoto, K.; Hiraide, T.; Mori, D.; Yamada, A.; Kanno, R.; Sonoyama, N.; Tamura, K.; Mizuki, J. *Electrochim. Acta* **2007**, *53*, 871–881.
(22) Hirayama, M.; Sonoyama, N.; Ito, M.; Minoura, M.; Mori, D.; Yamada, A.; Tamura, K.; Mizuki, J.; Kanno, R. *J. Electrochem. Soc.* **2007**, *154*, A1065–A1072.

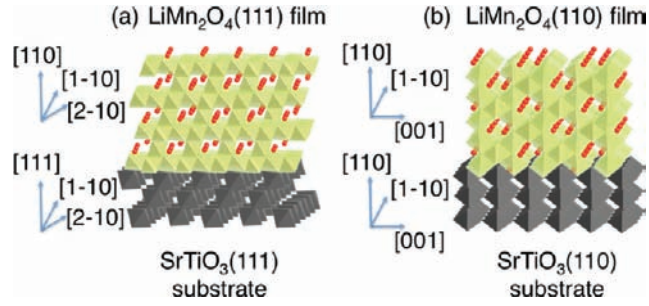

Figure 1. Lattice orientations of $LiMn_2O_4$ epitaxial thin films deposited on $SrTiO_3$ (111) and (110) substrates.

2. Experimental Section

Epitaxial $LiMn_2O_4$ thin films were grown on $SrTiO_3$ (111) and (110) substrates using a KrF excimer laser with a wavelength of 248 nm and a PLD system (PLD 3000, PVD Products Inc.). The synthesis conditions and the characterization results obtained by *ex situ* XRD, X-ray reflectivity (XRR; ATX-G, Rigaku), and atomic force microscopy (Nanoscope IIIa, Digital Instruments Inc.) for $LiMn_2O_4$ thin films with a highly flat surface have been described in detail elsewhere.[22] Figure 1 summarizes the orientations of the deposited $LiMn_2O_4$ films.

In situ XRD was performed using a κ-type six-circle diffractometer (New Port) installed on the bending-magnet beamline BL14B1 at SPring-8. The X-rays were monochromated by a Si(111) double-crystal system and focused by two Rh-coated bent mirrors. The dimensions of the incident X-ray beam were 0.1 mm (vertical) × 0.4−1.0 mm (horizontal; it was adjusted by a slit installed in front of the sample). The angular acceptance of the receiving slit was 2 mrad in the 2θ direction and 20 mrad in the χ direction. A wavelength of 0.82552 Å (15 keV) was selected. The *in situ* spectroelectrochemical cell designed for our experiments provided continuous structural changes with electrochemical lithium intercalation and deintercalation.[20−22] The counter electrode of the electrochemical cell was lithium metal, and the electrolyte solution was ethylene carbonate (EC)/diethyl carbonate (DEC) with a molar ratio of 3:7 in 1 M $LiPF_6$. The cell voltage was increased from the initial voltage to 5.0 V and was then reduced to 2.0 V. As the *in situ* electrochemical cell exhibits a large overpotential, a potential of 5.0 V was applied to the thin-film electrodes to promote the electrochemical reaction of Mn^{3+} to Mn^{4+} in $LiMn_2O_4$. This reaction was potentiostatically controlled using a potentiostat/galvanostat (Hokuto Denko, HA-501). Once the cell potential had stabilized, in- and out-of-plane XRD measurements were performed to investigate structural changes perpendicular and parallel to the substrate, respectively. After the measurements, the cell potential was changed to a fixed value for the next measurement.

For the *in situ* XRD measurements, we used a reciprocal coordinate system (H,K,L) with two components (H and K) parallel to the surface and the third component (L) normal to the surface; this reciprocal coordinate system is generally used for surface diffraction techniques. Reciprocal lattice space models for the (111) and (110) substrates are shown in the Supporting Information (Figure S1). The reciprocal lattice space model is described by cubic and hexagonal systems for $LiMn_2O_4(111)/SrTiO_3(111)$. The relationship between $(H,K,L)_{hexa}$ and $(h,k,l)_{cubic}$ (for the hexagonal and cubic lattices, respectively) is given by the transformations $H = h - k$, $K = k - l$, and $L = h + k + l$. Four diffraction peaks were observed for the $LiMn_2O_4$ (111) film: $(0,0,3)_{hexa}$, $(4,0,4)_{hexa}$, $(8,-4)_{hexa}$, and $(12,0)_{hexa}$. The reciprocal lattice space model is described by the cubic and tetragonal systems for $LiMn_2O_4(110)/SrTiO_3(110)$. The relationship between $(H,K,L)_{tetra}$ and $(h,k,l)_{cubic}$ (for the tetragonal and cubic lattices, respectively) is given by the transformations $H = l$, $K = h - k$, and $L = h + k$. Six diffraction peaks, $(1,0,2)_{tetra}$, $(0,0,8)_{tetra}$, $(0,4,4)_{tetra}$, $(4,0)_{tetra}$, $(0,8)_{tetra}$, and $(1,2)_{tetra}$, were observed for the $LiMn_2O_4$ (110) film. XRD patterns were

Table 1. Parameters Obtained by the Refinement of X-ray Reflectivity Data for As-Grown $LiMn_2O_4$ (111) and (110) Films Used for *in Situ* XRD Measurements

		surface impurity layer	$LiMn_2O_4$	$SrTiO_3$
$LiMn_2O_4$(111)	density d [g cm^{-3}]	2.01(9)	4.22(4)	5.12
	thickness l [nm]	1.12(8)	7.32(3)	–
	roughness t [nm]	0.58(8)	1.38(8)	1.01(6)
$LiMn_2O_4$(110)	density d [g cm^{-3}]	2.02(4)	4.13(4)	5.12
	thickness l [nm]	0.8(2)	4.84(5)	–
	roughness t [nm]	0.45(5)	1.50(4)	2.53(5)

obtained by an out-of-plane technique for (H,K,L) reflections ($L \neq 0$) and by an in-plane technique for (H,K) reflections ($L = 0$).

TEM observations were performed in the cross-sectional geometry for $LiMn_2O_4$ thin films after electrochemical cycling. Samples were coated with a carbon protective film by vacuum deposition. The samples were cut along the $(1\bar{1}0)$ planes of the $SrTiO_3$ substrate and thinned to electron transparency using a 30 kV Ga-ion beam (FEI Co., Dual Beam System Nova-200 Nanolab) at 30 kV. To avoid artifactual contributions due to the TEM sample preparation, the samples were cleaned using a low-intensity Ga-ion beam at a low accelerating voltage of 5 kV and then cleaned using a plasma cleaner prior to analysis. TEM observations were performed with a transmission electron microscope (JEOL Co., JEM-2100F) operating at 200 kV with a field-emission gun electron source. Electrochemical measurements were performed between 3.5 and 4.5 V for 10 cycles using the same electrochemical cell as that used for the *in situ* XRD measurements.

3. Results and Discussion

3.1. Synthesis and Characterization of Epitaxial Films. $LiMn_2O_4$ thin films were epitaxially grown on $SrTiO_3$ (111) and (110) substrates. The films have the same orientations as the substrate and were indexed as $LiMn_2O_4$ (111) and $LiMn_2O_4$ (110) (see Figure 1). The orientations, thicknesses, densities, and roughnesses of the epitaxial films were characterized by thin-film XRD and XRR, as shown in the Supporting Information (Figures S2 and S3). Table 1 summarizes the XRR results for the thin films used for *in situ* XRD measurements. The lattices of the $LiMn_2O_4$ epitaxial films were slightly distorted due to the lattice mismatch between the thin films and the $SrTiO_3$ substrates (7%). In this study, the distorted spinel is regarded as a pseudocubic lattice for simplicity. For the $LiMn_2O_4$ (111) film, the lattice parameters along the [111] and $[1\bar{1}0]$ directions (parallel and normal to the substrate, respectively) were 8.195(2) and 8.283(7) Å in a cubic lattice, respectively. For the $LiMn_2O_4$ (110) film, the lattice parameters along the [110], $[1\bar{1}0]$, and [001] directions were 8.247(2), 8.288(3), and 8.148(3) Å, respectively. The thicknesses and surface roughnesses of the epitaxial $LiMn_2O_4$ films were 7.32 and 0.58 nm for the (111) orientation and 4.84 and 0.45 nm for the (110) orientation, respectively. A surface layer with a density of 2.0 g cm^{-3} was detected, indicating the formation of impurity phases such as Li_2CO_3 (d = 2.1 g cm^{-3}) and LiOH (d = 1.4 g cm^{-3}) due to interfacial reactions of lithium in the film with moisture and carbon dioxide in air.[22] Using epitaxial $LiMn_2O_4$ thin films with sufficiently flat surfaces for surface scattering and electrochemical activity measurements has several advantages over using polycrystalline electrodes to elucidate surface phenomena at the electrode/electrolyte interface during battery operation.

3.2. *In Situ* X-ray Diffraction Measurements. Surface Structural Changes of $LiMn_2O_4$ (111). Figure 2 shows *in situ* XRD patterns of a pristine $LiMn_2O_4$ (111) film (dry) after the construction of a Li cell (OCV) and during the first charge–discharge process. The d values did not change significantly between 3.0 and 5.0 V. For example, the d value of the (0,0,3) reflection was 4.736(2) Å at OCV and 4.733(2) Å at 5.0 V. The structural changes observed in the $LiMn_2O_4$ epitaxial films exhibited extremely small, continuous lattice changes between 3.5 and 5.0 V. During the lithium (de)intercalation process, the phase transitions during intercalation and deintercalation of polycrystalline $Li_xMn_2O_4$ proceed via two steps of a single-phase reaction for $1 \geq x \geq 0.5$ and via two-phase reactions in the 4 V plateau region ($0.5 \geq x \geq 0$).[8,13,14] There are two main reasons for the structural changes of the epitaxial $LiMn_2O_4$ electrodes. First is the restriction of the $LiMn_2O_4$ lattice by the $SrTiO_3$ substrate. The lattice change and phase transformation in the $LiMn_2O_4$ epitaxial films may have been strongly constrained by the $SrTiO_3$ substrate, which caused a small lattice expansion or shrinkage and no phase transition during lithium (de)intercalation. Second, a nanoscale effect has been reported for nanoparticles of the electrode materials; this effect is related to the short diffusion length of lithium ions and electron transfer, the high surface reactivity due to the large contact area with the electrolyte, and the lower physical strains by lithium (de)intercalation.[23,24] These factors cause nanoparticles to exhibit a larger solid solution region and faster lithium ion diffusion

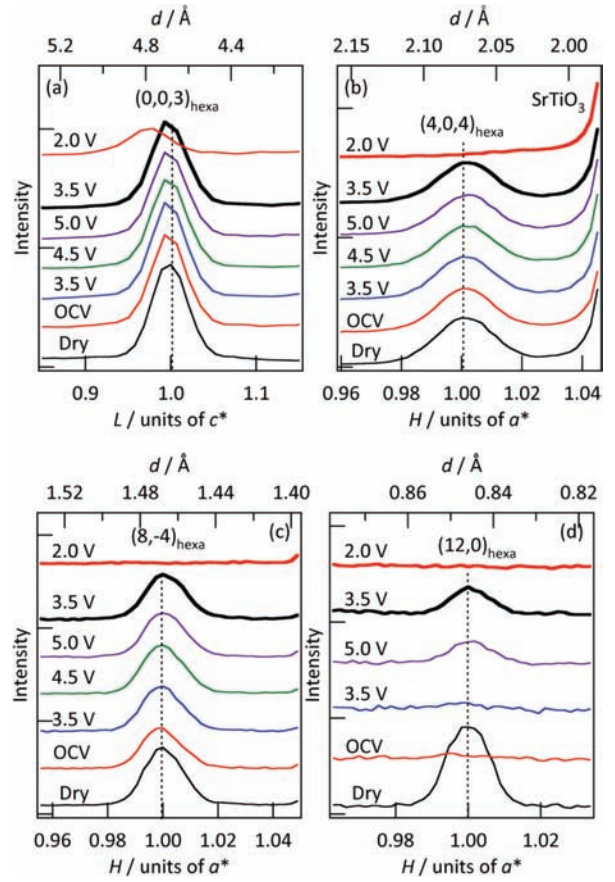

Figure 2. *In situ* XRD patterns for $LiMn_2O_4$ (111) during the first charge–discharge cycle. (a) $(0,0,3)_{hexa}$, (b) $(4,0,4)_{hexa}$, (c) $(8,-4)_{hexa}$, and (d) $(12,0)_{hexa}$ reflections. The $(0,0,3)_{hexa}$, $(4,0,4)_{hexa}$, $(8,-4)_{hexa}$, and $(12,0)_{hexa}$ peaks are attributed to the 111, 400, $4\bar{4}0$, and $8\bar{4}4$ peaks of $LiMn_2O_4$ using the original cubic lattice system.

(23) Wagemaker, M.; Borghols, W. J. H.; Mulder, F. M. *J. Am. Chem. Soc.* **2007**, *129*, 4323–4327.
(24) Zhou, H. S.; Li, D. L.; Hibino, M.; Honma, I. *Angew. Chem., Int. Ed.* **2005**, *44*, 797–802.

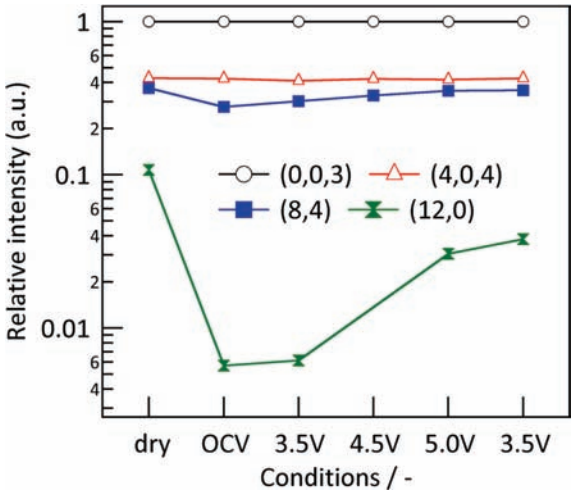

Figure 3. Peak intensity changes of $LiMn_2O_4$ (111) during the first charge−discharge cycle. $(0,0,3)_{hexa}$ $(4,0,4)_{hexa}$, $(8,-4)_{hexa}$, and $(12,0)_{hexa}$ reflections. The $(0,0,3)_{hexa}$, $(4,0,4)_{hexa}$, $(8,-4)_{hexa}$, and $(12,0)_{hexa}$ peaks are attributed to the 111, 400, 440, and 844 peaks of $LiMn_2O_4$ using the original cubic lattice system.

than microparticles. The very low thickness of the epitaxial films could be responsible for the single-phase reaction observed in our $LiMn_2O_4$ films. At 2.0 V, the $(0,0,3)_{hexa}$ diffraction peak shifted to a lower scattering vector, and no other peaks were observed in the angular range measured in the present study. The $LiMn_2O_4$ lattice expanded with lithium intercalation through the (111) surface below 3.0 V, indicating a phase transition from cubic $LiMn_2O_4$ to tetragonal $Li_2Mn_2O_4$. This phase transition is known to occur in polycrystalline $LiMn_2O_4$ spinel and is induced by Jahn−Teller distortion of $Mn^{III}O_6$ octahedra below 3.0 V.[6,25] The Jahn−Teller distortion might generate stress in the epitaxial lattice and permit lattice changes with the phase transition against the restriction imposed by the $SrTiO_3$ substrate.

Figure 3 shows the relative intensity variations of $(0,0,3)_{hexa}$, $(4,0,4)_{hexa}$, $(8,4)_{hexa}$, and $(12,0)_{hexa}$ diffraction peaks for the $LiMn_2O_4$ (111) epitaxial film before and during the first charge−discharge process. Each intensity was obtained by fitting a Gaussian curve, and the intensities were normalized using the value of the $(0,0,3)_{hexa}$ diffraction at all conditions. To discuss the intensity changes during the *in situ* XRD measurements, it is important to account for X-ray absorption by the electrolyte. This absorption reduces the diffraction peak intensity; this absorption is especially large for in-plane diffraction peaks because X-rays travel a considerable distance through the electrolyte at low incidence angles. Therefore, we kept the electrolyte volume in the electrochemical cell constant during these measurements. The peak intensities decreased when the electrode contacted the electrolyte in the $LiMn_2O_4$/EC + DEC/Li cell (OCV). The $(8,4)_{hexa}$ and $(12,0)_{hexa}$ diffraction peaks, which were measured by the in-plane technique using a low incident angle, exhibited larger reductions in peak intensity than the $(0,0,3)_{hexa}$ and $(4,0,0)_{hexa}$ diffraction peaks obtained by the out-of-plane measurement. During the first charge−discharge process, the relative intensities of the $(0,0,3)_{hexa}$ and $(4,0,0)_{hexa}$ diffraction peaks remained constant with increasing applied voltage, whereas those of the $(8,4)_{hexa}$ and $(12,0)_{hexa}$ diffraction peaks increased with increasing applied voltage. The relative intensities of diffraction peaks with low *d* values exhibited a large reduction and a large increase during electrolyte soaking and the electrochemical process, respectively. In contrast, the full width at half-maximum (fwhm) remained almost constant between 3.0 and 5.0 V (e.g., it was 0.028 for $(0,0,3)_{hexa}$), which indicates that the coherence domain length of the $LiMn_2O_4$ surface does not change during the intercalation and deintercalation processes. The fact that the relative intensity changes while the coherence domain length remains constant suggests that the atomic arrangements of the $LiMn_2O_4$ surface lattice change during the initial reaction process. At 2.0 V, the $(0,0,3)_{hexa}$ diffraction peak intensity decreased dramatically (Figure 2a), and the fwhm increased from 0.028 to 0.034. The lattice changes induced by Jahn−Teller distortion might destroy the crystals due to the large volume changes and the smaller domain size of $LiMn_2O_4$.

Surface Structural Changes of $LiMn_2O_4$ (110). Figure 4 shows *in situ* XRD patterns of the $LiMn_2O_4$ (110) epitaxial film before and during the first charge−discharge process. The $LiMn_2O_4$ (110) epitaxial film exhibited greater lattice changes than the $LiMn_2O_4$ (111) film. These larger lattice changes might be due to the poor epitaxy of the $LiMn_2O_4$ (110) film due to the greater interfacial roughness between $LiMn_2O_4$ (110) and $SrTiO_3$ (2.53 nm) than between $LiMn_2O_4$ (111) and $SrTiO_3$ (1.01 nm) (see Table 1). The *d* values of the $(0,0,8)_{tetra}$ and $(4,0)_{tetra}$ reflections were lower for dry conditions than for OCV (3.2 V) conditions, whereas the opposite trend was observed for the $(0,8)_{tetra}$ reflection. This result implies that surface structural changes occur during the initial reaction before electrochemical cycling. During the first charge−discharge process, the *d* values of the $(1,0,2)_{tetra}$, $(0,0,8)_{tetra}$, and $(0,4,4)_{tetra}$ reflections, which correspond to the out-of-plane structure, decreased when the applied voltage was increased from 3.2 to 5.0 V and increased when the applied voltage was reduced from 5.0 to 3.2 V. For the in-plane structures, the *d* value of the $(4,0)_{tetra}$ reflection increased, whereas those of the $(0,8)_{tetra}$ and $(1,2)_{tetra}$ reflections decreased. These results indicate that anisotropic lattice changes occur in the $LiMn_2O_4$ (110) epitaxial thin-film electrode. A new peak appeared at $d = 5.48$ Å along the $[H, 2H]_{tetra}$ direction that could not be indexed by the original $LiMn_2O_4$ spinel and tetragonal $Li_2Mn_2O_4$ lattices. A phase transition of a portion of the $LiMn_2O_4$ spinel occurred at the surface. From 3.2 to 2.0 V, the $(1,0,2)_{tetra}$ and $(0,0,8)_{tetra}$ diffraction peaks shifted to a lower scattering vector, whereas the $(4,0)_{tetra}$ peak shifted to a higher scattering vector; the other peaks were not detected in the measured angular range. These changes correspond to a phase transition from cubic to tetragonal $Li_{1+x}Mn_2O_4$. This behavior of the phase transition of the $LiMn_2O_4$ (110) film is similar to that of the $LiMn_2O_4$ (111) film.

Figure 5 shows relative intensity changes of the $LiMn_2O_4$ (110) epitaxial film before and during the first charge−discharge process. Each intensity was obtained by fitting a Gaussian curve, and the intensities were normalized using the $(1,0,2)_{tetra}$ diffraction intensity for all conditions. The peak intensities decreased when the electrode contacted the electrolyte in the $LiMn_2O_4$/EC + DEC/Li cell due to absorption of grazing-incidence X-rays, especially for the in-plane $(4,0)_{tetra}$, $(0,8)_{tetra}$, and $(1,2)_{tetra}$ reflections. The peak intensities of the $(4,0)_{tetra}$ and $(0,8)_{tetra}$ diffractions increased again during the first charge−discharge process on varying the applied voltage from 3.5 to 5.0 V and then from 5.0 to 3.5 V. No changes were observed in the peak intensities of the $(0,0,8)_{tetra}$, $(0,4,4)_{tetra}$, and $(1,2)_{tetra}$ diffractions, and a new reflection appeared. The fwhm of the

(25) David, W. I. F.; Thackeray, M. M.; Depicciotto, L. A.; Goodenough, J. B. *J. Solid State Chem.* **1987**, *67*, 316–323.

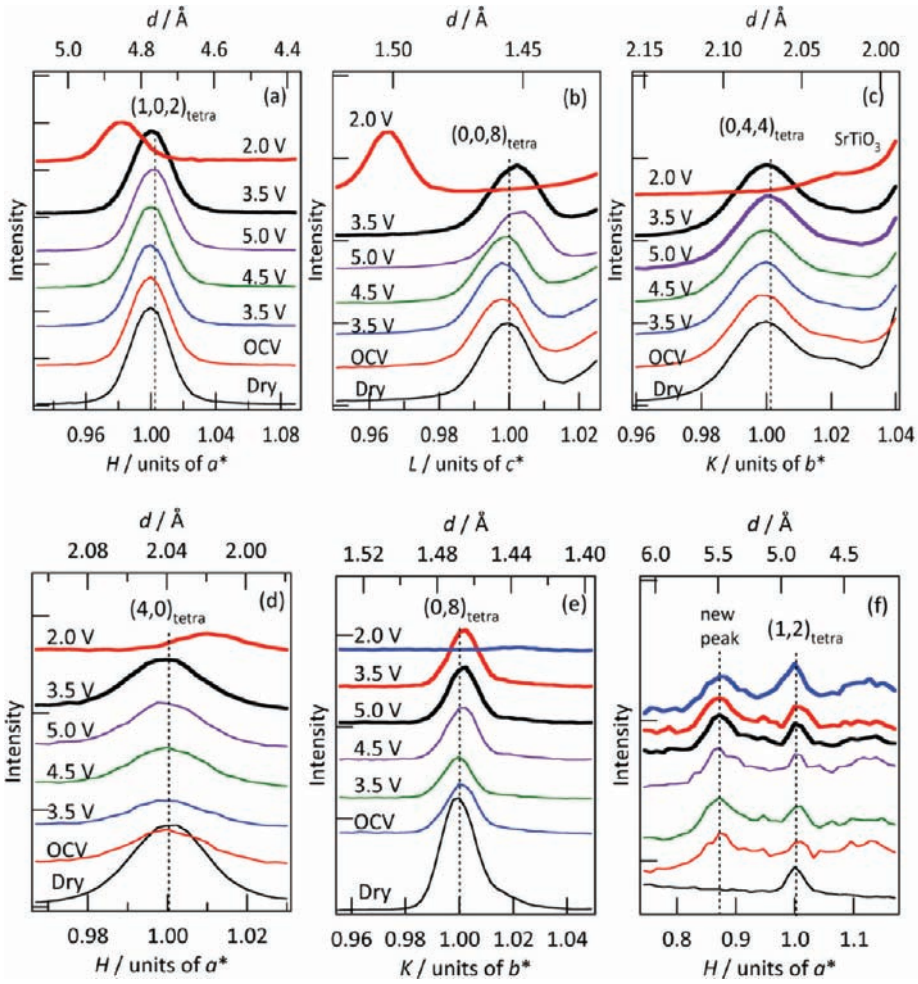

Figure 4. *In situ* XRD patterns of $LiMn_2O_4$ (110) during the first charge−discharge cycle. (a) $(1,0,2)_{tetra}$, (b) $(0,0,8)_{tetra}$, (c) $(0,4,4)_{tetra}$, (d) $(4,0)_{tetra}$, (e) $(0,8)_{tetra}$, and (f) $(1,2)_{tetra}$ reflections. The $(1,0,2)_{tetra}$, $(0,0,8)_{tetra}$, $(0,4,4)_{tetra}$, $(4,0)_{tetra}$, $(0,8)_{tetra}$, and $(1,2)_{tetra}$ peaks are attributed to the 111, 440, 400, 004, 440, and 111 peaks of $LiMn_2O_4$ using the original cubic lattice system.

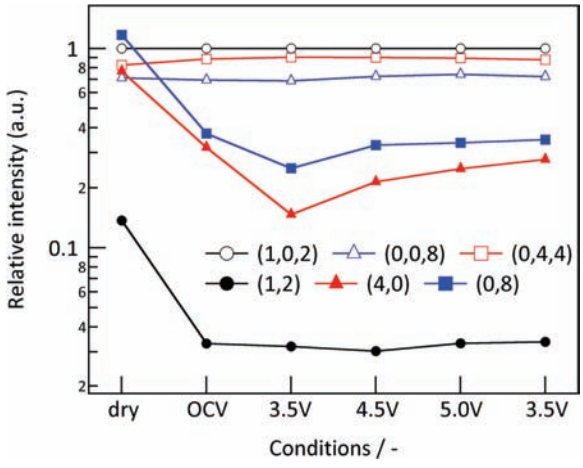

Figure 5. Relative intensity changes of $(1,0,2)_{tetra}$, $(0,0,8)_{tetra}$, $(0,4,4)_{tetra}$ $(4,0)_{tetra}$, $(0,8)_{tetra}$, and $(1,2)_{tetra}$ reflections of $LiMn_2O_4$ (110) during the first charge−discharge cycle. The $(1,0,2)_{tetra}$, $(0,0,8)_{tetra}$, $(0,4,4)_{tetra}$, $(4,0)_{tetra}$, $(0,8)_{tetra}$, and $(1,2)_{tetra}$ peaks are attributed to the 111, 440, 400, 004, 440, and 111 peaks of $LiMn_2O_4$ using the original cubic lattice system.

six diffraction peaks (e.g., 0.016 for $(1,0,2)_{tetra}$) remained almost constant from OCV to 5.0 V and from 5.0 to 3.0 V.

Structural Models of $LiMn_2O_4$ Surface. It is noteworthy that dramatic changes in the peak intensities of surface diffractions were observed for both the (111) and (110) planes of $LiMn_2O_4$ during electrolyte soaking and that a new reflection appeared in the (110) plane. The crystal structure of the $LiMn_2O_4$ surface suddenly changes before electrochemical cycling. As no changes in the lattice volume or the coherent domain length were observed, the atomic positions and/or site occupancy of $LiMn_2O_4$ on the electrolyte could differ from those of the original spinel lattice. It is reasonable that the atomic arrangement of the surface is modified when an electric double layer forms. To investigate how the atomic arrangement changes, the peak intensities of $LiMn_2O_4$ were simulated using structural models with different atomic positions from the $LiMn_2O_4$ spinel. The diffraction peak intensities should depend principally on the displacement of Mn atoms, which have a larger atomic scattering factor than Li or O atoms. Therefore, we conjecture that the structure consists of a $LiMn_2O_4$ lattice in which the Mn atoms are displaced from the 16d site (see Figure S5). Additionally, structural models that account for site occupancies are unable to explain the observed changes in the diffraction peak intensities. Figure 6 shows the relative intensities of the 111, 400, 440, and 844 diffraction peaks of $LiMn_2O_4$ for four different locations of Mn atoms. The intensities are normalized using the value of the (111) diffraction peak for all conditions. The relative intensities of peaks with low *d* values decrease as the Mn atom displacements increase. This behavior is consistent with the intensity

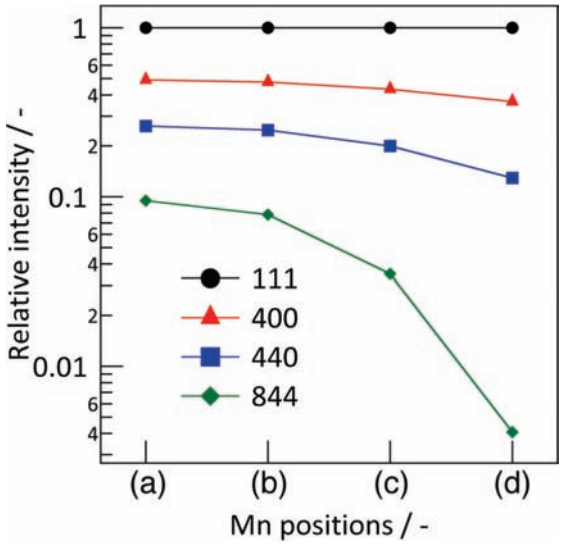

Figure 6. Relative intensities of 111, 400, 440, and 844 diffraction peaks of XRD patterns of $LiMn_2O_4$ simulated using four different Mn positions, (a) (1/2, 1/2, 1/2) (16d: original spinel), (b) (0.50, 0.51, 0.51), (c) (0.50, 0.51, 0.53), and (d) (0.50, 0.51, 0.55).

changes for $LiMn_2O_4$ (111) and (110) epitaxial thin films observed in this study. These results indicate that the changes in the peak intensities that occur during electrolyte soaking are due to a reduction in the symmetry of the atoms on the electrode surface.

A considerable amount is known about surface structural changes that occur at certain ideal interfaces. Since atoms in the surface plane are subject to interatomic forces in only one direction, the force imbalance alters the atomic positions near the surface so that surface atoms have different spacings and/or symmetries from bulk atoms. For example, adsorption of oxygen on clean germanium surfaces displaces surface atoms from the bulk lattice positions.[26] Surface structural studies on ideal surfaces have demonstrated that surface structures minimize the surface energy, so that they differ from bulk structures. For solid/liquid interfaces, *in situ* X-ray surface scattering has revealed the surface-phase transitions of a Bi monolayer electrodeposited on a Au (111) single crystal.[27] Surface structures at electrochemical interfaces are thought to vary with the adsorption species and to significantly affect the electrode reaction. Like the surface structures of these ideal systems, the $LiMn_2O_4$ surface structure differs from the bulk structure. Changes in atomic positions resulting in a reduction in symmetry were observed immediately after the $LiMn_2O_4$ electrode was soaked in the electrolyte. Surface structural changes could accompany ion diffusion and/or a change in the adsorption species at the electrode/electrolyte interface due to the formation of the electric double layer.

3.3. TEM Observations of Cycled $LiMn_2O_4$ Films. The surface morphologies of $LiMn_2O_4$ (111) and (110) films were investigated by high-resolution TEM (HR-TEM). Both the pristine $LiMn_2O_4$ (111) and (110) films exhibited sharp interfaces with the $SrTiO_3$ (111) and (110) substrates, respectively, and had a flat top surface and a uniform structure that did not vary from the surface to the bulk. Figure 7a shows a cross-sectional HR-TEM image of the surface of a 38-nm-thick

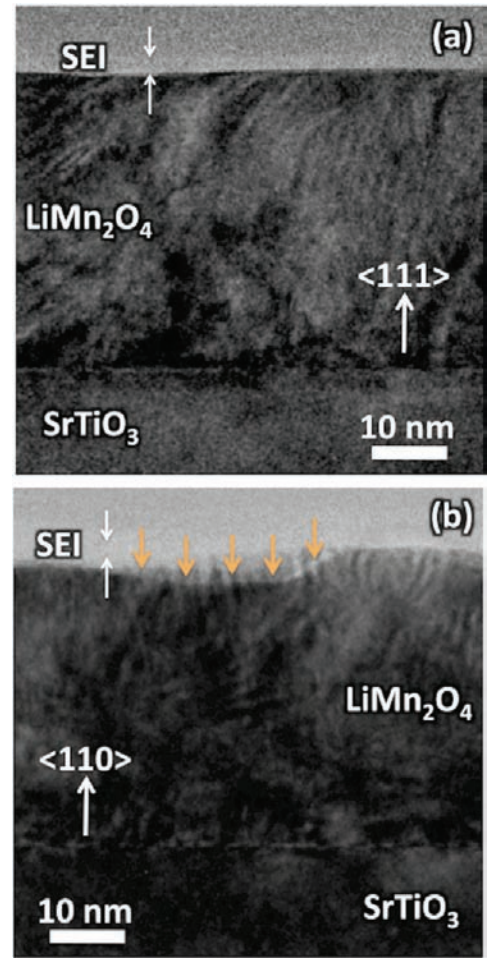

Figure 7. Cross-sectional bright-field TEM images of epitaxial $LiMn_2O_4$ (a) (111) and (b) (110) films after electrochemical 10 cycles.

$LiMn_2O_4$ (111) film that had been subjected to electrochemical cycling. The viewing direction of this image is along the $[1\bar{1}0]$ in-plane direction of the $SrTiO_3$ (111) substrate. The cycled $LiMn_2O_4$ (111) film exhibited a flat, planar surface. No contrast variation was observed from the surface to a depth of 10 nm. A dense and flat solid electrolyte interface (SEI) layer was formed on the surface. This result demonstrates the surface stability of the (111) plane during the electrochemical process. Figure 7b shows a cross-sectional HR-TEM image of the surface of the $LiMn_2O_4$ (110) film after electrochemical cycling. The viewing direction was along the $[1\bar{1}0]$ in-plane direction of the $SrTiO_3$ (110) substrate. Although the SEI layer also formed on the (110) surface, the cycled $LiMn_2O_4$ (110) film exhibited a rough top surface with a 20 nm $\times$5 nm pit. Furthermore, the contrast varied from the surface to a depth of 10 nm, which indicates that incoherent strains were generated in the electrochemical process. These TEM results for the (111) and (110) films demonstrate the dependence of the surface structure of $LiMn_2O_4$ on the lattice plane. The TEM observations also indicate that the (111) plane is more stable than the (110) plane during the electrochemical process.

3.4. Discussion. Surface Reconstruction of $LiMn_2O_4$. Most previous studies of the $LiMn_2O_4$ electrode surface were based on *ex situ* techniques under accelerated aging conditions using polycrystalline materials, and they mainly investigated the composition and structure of the SEI phase formed at the electrode/electrolyte interface. X-ray photoelectron spectros-

(26) Schlier, R. E.; Farnsworth, H. E. *J. Chem. Phys.* **1959**, *30*, 917–926.
(27) Tamura, K.; Wang, J. X.; Adzic, R. R.; Ocko, B. M. *J. Phys. Chem. B* **2004**, *108*, 1992–1998.

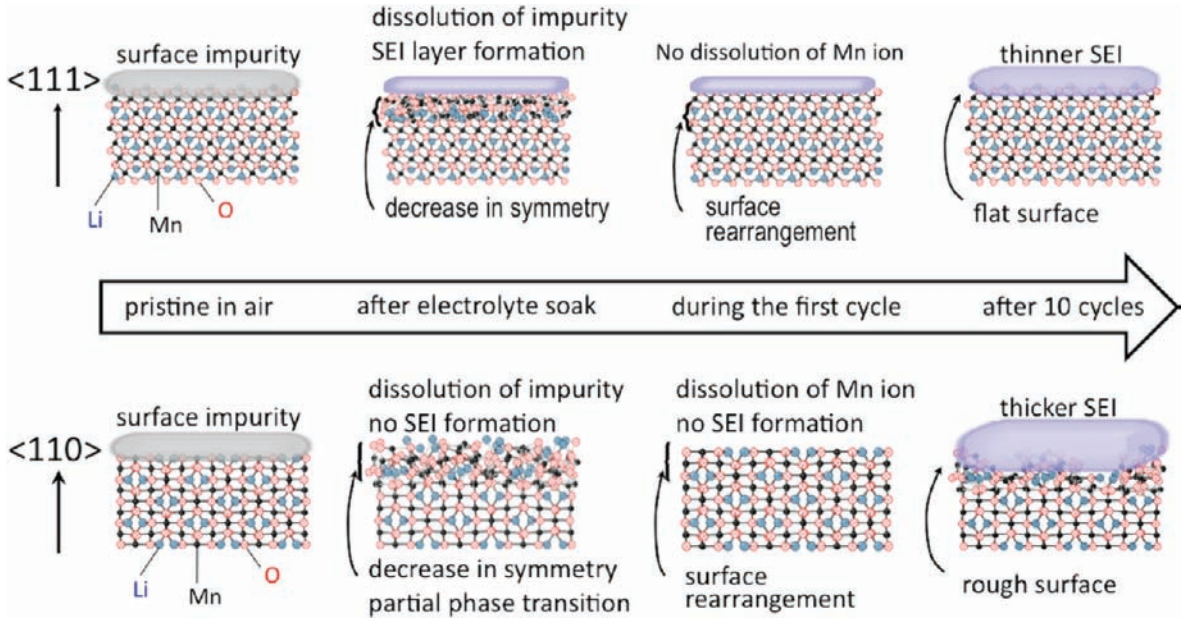

Figure 8. Schematic of surface reactions for (111) and (110) crystal planes of $LiMn_2O_4$ characterized by *in situ* XRD and XRR measurements and *ex situ* TEM observations.

copy[28,29] and Fourier transform infrared spectroscopy[28] confirmed the formation of an SEI layer on the $LiMn_2O_4$ electrode surface after several charge−discharge cycles. McLarnon et al. reported that SEI layer formation was accompanied by conversion of the original $LiMn_2O_4$ into α-MnO_2 in an EC-DMC-$LiPF_6$ electrolyte.[29] The SEI layer increases the calendar life of lithium batteries because it provides protection from acidic solution species. Like an SEI layer, an oxide coating on the surface layer can increase the cyclability of batteries.[30,31] In terms of power characteristics, electrochemical studies revealed that the desolvation process was the rate-determining step of the electrode reaction.[32−34] Although these spectroscopic and electrochemical analyses demonstrated the importance of the SEI layer, the calendar life and power characteristics of batteries depend on both the SEI phase and the surface structure of the electrode itself. Therefore, the crystal structures of the electrode surface during battery operation need to be clarified to elucidate the detailed interfacial reactions of lithium batteries. However, the surface structural changes remain unclear. The present study clarified the surface structures by *in situ* SXRD and *ex situ* TEM using epitaxial $LiMn_2O_4$ thin films. The $LiMn_2O_4$ surface exhibited drastic structural changes during the initial electrochemical process. Figure 8 summarizes the surface structures and surface reactions of $LiMn_2O_4$ (111) and (110) films observed by *in situ* XRD, *ex situ* TEM, and *in situ* XRR[22] measurements.

In situ SXRD measurements reveal drastic changes in the atomic arrangements with a reduction in symmetry at the electrode surface after soaking in the electrolyte. When the electrode contacts the electrolyte, electrons in the electrode and solvent ions in the electrolyte generally move to form an electric double layer. For intercalation materials, lithium ions can also migrate between the electrode surface and the electrolyte due to their different lithium concentrations. *In situ* XRR has revealed that impurity phases form on the pristine (111) and (110) planes due to reactions with moisture and carbon dioxide in ambient air during the initial process, and an SEI layer forms on the (111) surface during electrolyte soaking.[22] These interfacial reactions could drive the surface structural changes. Whereas atomic rearrangement is common to both the (111) and (110) surfaces, a stable surface structure during electrolyte soaking depends on the lattice plane. The relative intensities of peaks with low d values ($(8,4)_{hexa}$ and $(12,0)_{hexa}$ for the (111) film and $(4,0)_{tetra}$ and $(0,8)_{tetra}$ for the (110) film) gradually increase as the applied voltage is increased above 3.5 V. Based on the simulated XRD patterns shown in Figure 7, the intensity change is considered to be associated with a recovery of the symmetry of Mn atoms. Rearrangement of the surface structure (i.e., surface reconstruction) occurs on both the (111) and (110) films during the first charge process. The relative intensities after the first discharge differ from those in dry conditions, even when X-ray absorption by the electrolyte is taken into account. Therefore, the atomic positions of the surface structure after the electrochemical process differ from the original atomic positions of the spinel structure. Surface reconstruction is generally induced by instability of the termination structure, and it depends on the surface energy of lattice planes. No published results are available for the $LiMn_2O_4$ surface, but the surface energies of the (111), (110), and (100) planes of $MgAl_2O_4$ with the spinel structure have been investigated by atomistic simulation.[35,36] The lowest surface energies for potential cleavage planes before reconstruction are 8.44, 5.25, and 4.00 $J \cdot m^{-2}$

(28) Aurbach, D.; Levi, M. D.; Levi, E.; Teller, H.; Markovsky, B.; Salitra, G.; Heider, U.; Heider, L. *J. Electrochem. Soc.* **1998**, *145*, 3024–3034.
(29) Matsuo, Y.; Kostecki, R.; McLarnon, F. *J. Electrochem. Soc.* **2001**, *148*, A687–A692.
(30) Eftekhari, A. *Solid State Ionics* **2004**, *167*, 237–242.
(31) Gnanaraj, J. S.; Pol, V. G.; Gedanken, A.; Aurbach, D. *Electrochem. Commun.* **2003**, *5*, 940–945.
(32) Yamada, I.; Abe, T.; Iriyama, Y.; Ogumi, Z. *Electrochem. Commun.* **2003**, *5*, 502–505.
(33) Abe, T.; Fukuda, H.; Iriyama, Y.; Ogumi, Z. *J. Electrochem. Soc.* **2004**, *151*, A1120–A1123.
(34) Ogumi, Z.; Abe, T.; Fukutsuka, T.; Yamate, S.; Iriyama, Y. *J. Power Sources* **2004**, *127*, 72–75.
(35) Davies, M. J.; Parker, S. C.; Watson, G. W. *J. Mater. Chem.* **1994**, *4*, 813–816.
(36) Fang, C. M.; Parker, S. C.; With, G. d.; Chen, L. Q. *J. Am. Ceram. Soc.* **2000**, *83*, 2082.

for the (111), (110), and (100) planes, respectively. Calculations reveal that surface reconstruction at the unstable (111) and (110) planes is accompanied by rearrangement of Mg and O atoms. Assuming that the $LiMn_2O_4$ surfaces have an order of stability similar to that of the $MgAl_2O_4$ surfaces, it is reasonable to assume that surface reconstruction of $LiMn_2O_4$ (111) and (110) films forms a stable termination structure in response to changes in the interfacial conditions due to the lithium (de)intercalation reactions. The absence of changes to the SXRD patterns after the first discharge reveals that the surface reconstruction at the $LiMn_2O_4$ surface occurs during the very early stages of battery operation. The SXRD patterns of the (111) and (110) films after reconstruction have the same diffraction peak positions but different intensity ratios. The reconstructed structures have similar lattice volumes, and the atomic arrangements differ according to the lattice plane. Our results represent the first experimental evidence for reconstruction of $LiMn_2O_4$ surfaces and lattice-plane anisotropy during the battery reaction. Since lattice changes in epitaxial $LiMn_2O_4$ films are restricted by the $SrTiO_3$ substrate, a polycrystalline $LiMn_2O_4$ surface with no restrictions might undergo more drastic structural changes during reconstruction.

We have investigated the surface structures and interfacial reactions of layered rock salt, $LiNi_{0.8}Co_{0.2}O_2$.[37] The surface structures of $LiNi_{0.8}Co_{0.2}O_2$ also collapse upon being soaked in an electrolyte and are reconstructed when a voltage is applied during the first charge process, but the reconstruction rate of $LiNi_{0.8}Co_{0.2}O_2$ is higher than that of $LiMn_2O_4$. No phase transition or dissolution of transition metals was observed for $LiNi_{0.8}Co_{0.2}O_2$ during the initial process. Although the surface structure of any intercalation material may change, the extent of these changes and the stability of the re-formed surface depend on both the lattice planes and the electrode material. The $LiMn_2O_4$ surface seems to be less stable than layered rock salt materials.

SEI Formation on $LiMn_2O_4$ Surface. *In situ* XRR revealed that the SEI phase on the (111) lattice plane grows during electrolyte soaking, whereas no SEI phase forms on the (110) plane (see Figure 8). The (111) plane is more readily covered with the SEI layer than the (110) plane during electrolyte soaking. In contrast, *ex situ* TEM images after 10 cycles reveal that an SEI layer grows on the (110) plane during the electrochemical process and that the SEI layer on the (110) plane (5−8 nm) is thicker than that on the (111) plane (3.5 nm). These results demonstrate that the reactivity of SEI formation on the $LiMn_2O_4$ surface depends on the reaction process. Like surface reconstruction, SEI formation could be induced on a lattice plane with a high surface energy. In the initial reaction process during electrolyte soaking, the higher surface energy of the (111) plane over the (110) plane is compatible with the higher reactivity of the SEI formation at the $LiMn_2O_4$ (111) plane. The (110) surface, which is more stable and less reactive, does not lead to SEI layer formation. In the initial reaction process, surface reconstruction proceeds simultaneously at the (111) and (110) planes; this might alter their surface energies and thus the surface stabilities. The reconstructed (110) surface could have a higher surface energy than the reconstructed (111) surface due to SEI formation during the electrochemical process on the (110) surface. The surface reactivity of $LiMn_2O_4$ with the electrolyte species changes with surface reconstruction.

(37) Sakamoto, K.; Hirayama, M.; Sonoyama, N.; Yamada, A.; Tamura, K.; Mizuki, J.; Kanno, R. *Chem. Mater.* **2009**, *21*, 2632–2640.

Effects of Surface Reconstruction on $LiMn_2O_4$ Stability. The $LiMn_2O_4$ (111) and (110) surfaces formed in ambient air are unstable in the electrolyte and on battery reaction, and surface reconstruction occurs to form a stable surface termination at the first charge process. As the reconstructed $LiMn_2O_4$ surface is the starting point of lithium (de)intercalation, SEI formation, and Mn dissolution, the reconstructed structure could strongly affect the stability of the electrode. We discuss the stability of $LiMn_2O_4$ during the initial charge process and during subsequent cycles after reconstruction.

The pristine (111) surface (which has the higher surface energy) is readily covered by the SEI layer, and no deterioration is detected during the first cycle.[22] In contrast, no SEI phase forms on the pristine (110) surface (which has the lower surface energy), and Mn dissolution occurs during the first charging.[22] The higher stability of the (111) plane over the (110) plane can be explained by two different hypotheses. The first hypothesis is that the SEI layer prevents the (111) surface from directly contacting the electrolyte, providing a more stable electrochemical interface than the (110) surface, which does not have a SEI layer. This is a well-known explanation for the improved electrode stability on SEI layer formation. The SEI layer reduces the deterioration rate of the $LiMn_2O_4$ surface, which is intrinsically unstable. The second hypothesis is that the intermediate reconstructed structure of the (111) plane is more resistant to Mn dissolution than the (110) plane. This interpretation implies that the stable reconstructed structure at the surface makes the electrode more stable.

After 10 cycles, a thicker SEI layer has grown on the (110) plane than on the (111) plane. However, *ex situ* TEM images of the (111) and (110) films reveal that the (111) surface is flat whereas the (110) surface is rough, indicating the deterioration from the (110) surface. In this process, surface stabilization by SEI formation is incompatible with the instability of the (110) surface. In contrast, the different stabilities of the reconstructed structures is a clear indication of the anisotropic stability of the (111) and (110) surfaces after the SEI layer has formed on both lattice planes. The reconstructed structure on the (111) surface is more stable during battery operations than the (110) surface. The instability of the reconstructed (110) surface is consistent with the thicker SEI phase, which occurs on the lattice plane with the higher surface energy. The surface stability of the $LiMn_2O_4$ electrode depends on the reconstructed structure that reduces the surface energy of the electrode surface on the electrochemical process.

It is important to determine why the reconstructed (111) surface is more stable than the (110) surface. The surface stability may be related to variations in the surface termination arrangements of oxygen ions and/or manganese ions with valence changes during battery reactions. However, the surface energies of the reconstructed structures of $LiMn_2O_4$ during the electrochemical process are unclear since it is difficult to perform atomic calculations that consider both electric double layer and lithium diffusion. Hence, we discuss the resistance of the electrode to Mn dissolution on the basis of atomic stacking of pristine $LiMn_2O_4$. Figure 9 shows the surface structures of $LiMn_2O_4$ (111) and (110) orientations. The (111) plane is terminated by a cubic closed-packed oxygen arrangement in the spinel structure, whereas no closed-packed arrangement of oxygen appears in the (110) plane. The oxygen ions at the $LiMn_2O_4$ surface are modified by species in the electrolyte (such as lithium and hydrogen ions) during electrolyte soaking. Manganese ions are arranged two-dimensionally in the ⟨111⟩

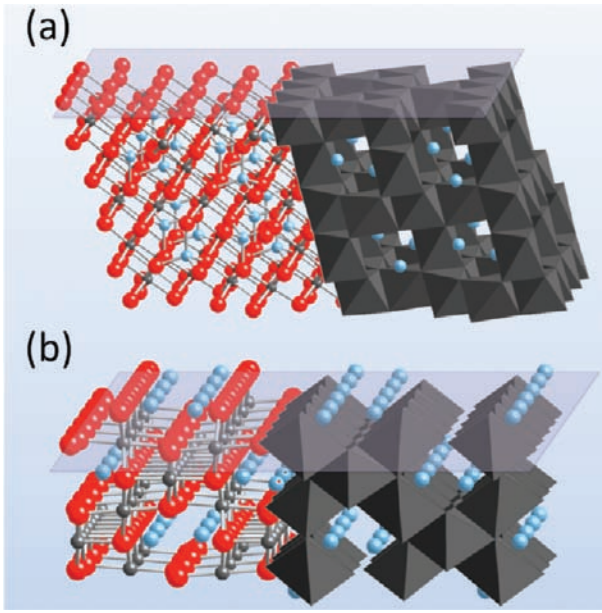

Figure 9. Atomic stackings of $LiMn_2O_4$ (a) (111) and (b) (110) orientations.

direction and one-dimensionally in the ⟨110⟩ direction. The manganese ions are less densely arranged at the (110) surface and are expected to be in close contact with the electrolyte. This structure makes the manganese ions highly reactive with solvents in the electrolyte, which is consistent with the (110) plane being less stable than the (111) surface. The arrangements of both oxygen and manganese ions could explain the lattice-plane dependence of the surface stability of $LiMn_2O_4$.

Many researchers have reported that surface modification by oxides such as ZnO, Al_2O_3, and ZrO_2 enhances the cycling stability of $LiMn_2O_4$.[18,38−43] Like the SEI phase, surface modification is believed to minimize the contact area of $LiMn_2O_4$ with the electrolyte and suppress the loss of manganese ions from the surface into the electrolyte. However, the SEI layer, which may separate the electrode surface from the electrolyte, could not prevent Mn dissolution at the $LiMn_2O_4$ (110) plane, whereas no significant deterioration was observed for the $LiMn_2O_4$ (111) plane. This indicates the importance of surface reconstruction on the electrode stability. It also implies that surface modification affects the electrode stability. Heat treatment at 300−800 °C after oxide coating improves the electrode stability.[44,45] The reacted surface, which has a different composition, might lead to a stable reconstructed structure during the electrochemical process, suppressing the phase transition and Mn dissolution. Surface reconstruction provides a new explanation for why surface modification by oxides improves the cyclability characteristics of $LiMn_2O_4$. Surface valence changes in manganese and oxygen ions during and/or after the electrochemical process should be investigated to provide complementary information for clarifying the manganese dissolution process and the deterioration mechanism of the lithium manganese oxide spinel. Further studies involving X-ray absorption near-edge structure and electron energy loss spectroscopy are currently underway.[46]

4. Concluding Remarks

$LiMn_2O_4$ epitaxial films with (111) and (110) orientations have been synthesized by PLD using $SrTiO_3$ (111) and (110) substrates, respectively. These epitaxial films have low roughnesses (about 2 nm) and provide a simple reaction field for electrochemical intercalation reactions. *In situ* surface X-ray diffraction measurements detect changes in the surface structure during the first charge−discharge process. This represents the first experimental demonstration that the $LiMn_2O_4$ surface has a different structure during battery operation than in the atmosphere. The atomic arrangements of the $LiMn_2O_4$ surface change on being soaked in the electrolyte and are subsequently reconstructed when a voltage is applied in the first charge process; this indicates an adjustment to the electrochemical reaction process. This reconstruction is common to the (111) and (110) surfaces. The surface structures vary not only due to Jahn−Teller distortion but also due to interfacial reactions such as the formation of an electric double layer, dissolution of the electrode, and formation of an SEI phase during lithium (de)intercalation. Although TEM images after 10 cycles reveal that the (110) plane is covered with a thicker SEI layer, it is less stable than the (111) plane. The electrode stability depends on the reconstructed structure at the surface. *In situ* X-ray surface diffraction using epitaxial thin-film electrodes was quite effective in revealing the reaction mechanism at the electrode surface of lithium ion batteries. The surface structural changes of the epitaxial films provide an example of surface changes in a material with a nanoscale thickness and a large lattice strain due to its substrate. On the basis of the large surface structural changes observed in substrate-restricted epitaxial $LiMn_2O_4$ films, we anticipate that the surfaces of practical $LiMn_2O_4$ electrodes will exhibit changes that are more drastic during battery operation than the restricted electrodes of this study. Mechanical and technical development of surface structures is of considerable importance for improving the power characteristics and cyclability of new-generation batteries.

Acknowledgment. This work was conducted as part of a collaboration program with the Genesis Research Institute. This work was partly supported by a Grant-in-Aid for Scientific Research (A) and a Grant-in-Aid for Young Scientists (B), Japan Society for the Promotion of Science. The synchrotron radiation experiments were performed as projects approved by the Japan Synchrotron Radiation Research Institute (JASRI) (Proposal No. 2006B1623).

Supporting Information Available: Figures S1−S5. This material is available free of charge via the Internet at http://pubs.acs.org.

JA105389T

(38) Amatucci, G.; Tarascon, J. M. *J. Electrochem. Soc.* **2002**, *149*, K31–K46.
(39) Amatucci, G. G.; Blyr, A.; Sigala, C.; Alfonse, P.; Tarascon, J. M. *Solid State Ionics* **1997**, *104*, 13–25.
(40) Amatucci, G. G.; Pereira, N.; Zheng, T.; Tarascon, J. M. *J. Electrochem. Soc.* **2001**, *148*, A171–A182.
(41) Kannan, A. M.; Manthiram, A. *Electrochem. Solid State Lett.* **2002**, *5*, A167–A169.
(42) Sun, Y. K.; Hong, K. J.; Prakash, J.; Amine, K. *Electrochem. Commun.* **2002**, *4*, 344–348.
(43) Fu, L. J.; Liu, H.; Li, C.; Wu, Y. P.; Rahm, E.; Holze, R.; Wu, H. Q. *Solid State Sci.* **2006**, *8*, 113–128.
(44) Kannan, A. M.; Manthiram, A. *Electrochem. Solid-State Lett.* **2002**, *5*, A167–A169.
(45) Sun, Y.; Wang, Z.; Chen, L.; Huang, X. *J. Electrochem. Soc.* **2003**, *150*, A1294–A1298.
(46) Hirayama, M.; Ido, H.; Kim, K.; Suzuki, K.; Kanno, R. 2010, submitted.